Role of hydrogen atoms in the photoinduced formation of stable electron centers in H-doped $12CaO \cdot 7Al_2O_3$

Peter V. Sushko* and Alexander L. Shluger
Department of Physics & Astronomy, University College London, Gower Street, London WC1E 6BT, United Kingdom

Katsuro Hayashi
Frontier Collaborative Research Center, P.O. Box S2-13, Tokyo Institute of Technology, 4259 Nagasuta, Midori-ku, Yokohama 226-8503, Japan

Masahiro Hirano
SORST, Japan Science and Technology Agency, P.O. Box S2-13, Tokyo Institute of Technology, 4259 Nagasuta, Midori-ku, Yokohama 226-8503, Japan

Hideo Hosono
Frontier Collaborative Research Center and Materials and Structures Laboratory, Tokyo Institute of Technology, 4259 Nagasuta, Midori-ku, Yokohama 226-8503, Japan

(Received 3 June 2005; revised manuscript received 13 September 2005; published 24 January 2006)

In this work we investigate a variety of chemical and photoinduced processes in which different hydrogenous species including H_2 molecules, H^- ions, and H^0 atoms interact with the bulk of a complex nanoporous oxide $12CaO \cdot 7Al_2O_3$. Our results provide a detailed and consistent explanation of the recently observed phenomenon of photoinduced conversion of the insulating H-doped $12CaO \cdot 7Al_2O_3$ to a conductor [K. Hayashi *et al.*, Nature (London) **419**, 462 (2002)]. The formation of a large and thermally stable concentration of electron centers in this process is facilitated by a large concentration (up to 10^{20} cm^{-3}) of extraframework O^{2-} naturally present in this material and homogeneously distributed in its bulk. We show that these species are able to split H_2 molecules into pairs of H^+ and H^- ions and convert H^0 atoms into H^+ and e^- promoting the photoinduced conversion process. The similarity of the mechanisms described in this work to those known for low-coordinated sites at MgO surfaces indicates that the formation of electronic centers in oxides interacting with hydrogenous species could be a generic feature.

DOI: 10.1103/PhysRevB.73.045120 PACS number(s): 61.72.Bb, 72.20.Jv, 61.72.Ji, 71.20.−b

I. INTRODUCTION

The properties of hydrogen in oxides have been in the focus of recent research (see, for example, Refs. 1–3 and references therein). The amphoteric behavior of hydrogen is one of its most intriguing features: depending on the environment it exhibits three charge states of H^+, H^0, or H^-. Gaining control over the mechanisms of hydrogen charge state interconversion and stabilization is important fundamentally and for future technological applications.

In this work we study the properties of hydrogenous species in a complex nanoporous oxide $12CaO \cdot 7Al_2O_3$ (C12A7). It has been experimentally established that hydrogencontaining C12A7 (C12A7:H) can be converted from its insulating, transparent, and diamagnetic state into a persistent electronic conductor. Simultaneously with the insulator-conductor transition the C12A7:H acquires a greenish color and begins to exhibit a strong paramagnetic signal due to the presence of unpaired electrons.[4]

We demonstrate that these changes involve all three hydrogen charge states (H^+, H^0, and H^-) and discuss in detail the mechanisms of interconversion between them induced by the uv irradiation of C12A7:H. We show that a large concentration of thermally stable electronic centers can be formed via photoionization of H^- species ($H^- + \hbar\nu \rightarrow H^0 + e^-$) and consequent relaxation of metastable H^0 atoms into a more energetically favorable configuration of H^+ and e^-. We also show that the interaction of hydrogenous species with C12A7 lattice ions plays a crucial role in this process. Analysis of parallels between the properties of hydrogenous species in bulk C12A7 and at the MgO surface suggests that the photoinduced formation of transient H^0 atoms and their conversion into a H^+ and e^- may be generic to oxides.

The paper is organized as follows. The complex structure of C12A7 and the main experimental results are described in Sec. II. Section III contains the details of the computations. The results of the theoretical calculations are presented in Sec. IV. The summary of the photoinduced processes in C12A7:H and the comparison with the experimental data are given in Sec. V. A possible generalization of our results to other oxides is discussed in Sec. VI. Finally, in the Appendix we consider the nature of the electronic centers in C12A7 using the periodic model. These results are consistent with the conclusions of our earlier studies[5,6] carried out using the embedded cluster approach and provide further support to the model presented in this work.

II. EXPERIMENTAL BACKGROUND

A. Description of the system

Many of the fascinating properties of C12A7 are thought to be associated with its unusual structure. C12A7 is a cubic

crystal, which belongs to the $I\bar{4}3d$ space group and has a lattice constant of 11.99 Å. The cubic unit cell contains two molecules of the $12CaO \cdot 7Al_2O_3$ composite which are arranged so that they form a positively charged framework built from densely packed cages with negative extraframework O^{2-} ions distributed over them. The overall structure can be represented by the chemical formula $[Ca_{24}Al_{28}O_{64}]^{4+} \cdot 2O^{2-}$, where $[Ca_{24}Al_{28}O_{64}]$ defines the *framework* containing 12 cages per unit cell with each cage surrounded by eight first-neighbor cages and four second-neighbor cages and the $2O^{2-}$ represent an example of the possible *extraframework* species. Other extraframework species such as OH^-, O_2^-, O^-, and F^- ions have also been reported.[7–12]

Two major features of the C12A7 lattice determine its properties. First, the framework is positively charged with the charge $+4e$ being distributed over 12 cages. The exact distribution of the positive charge is difficult to characterize. However, in the absence of additional information, we assume the charge of the framework is distributed homogeneously, i.e., a charge of $+(1/3)e$ per cage can be associated with the wall of each cage [see Fig. 1(a)]. The compensating negative charge is provided by so-called extraframework species such as O^{2-}, which are thought to be randomly, but on average homogeneously, distributed over the lattice and occupy sites in the middle of the cages. Second, since the extraframework oxygen ions occupy only one cage out of six, they will tend to maximize the distance between themselves due to their electrostatic repulsion.[13] However, even in this case the extraframework O^{2-} are separated by no more than 10 Å and for most cages at least one of the neighboring cages will be occupied by an O^{2-} ion. The number of neighboring extraframework species increases if doubly charged extraframework species, such as O^{2-} ions, are replaced with singly charged species, such as O^- or OH^-. This inevitably modifies the details of the lattice structure and the relative arrangement of the extraframework ions as well as the electrostatic potential and consequently affects the properties of the framework and extraframework species.

A single cage of C12A7 is shown in Fig. 1(a). It contains six Ca, eight Al and 16 O ions forming the cage wall. It is important to point out that although all Ca sites in the bulk C12A7 are equivalent, there are two types of Ca sites with respect to each cage. In particular, two Ca ions, indicated as Ca(I) in Fig. 1(a), occupy the sites on the opposite sides of the cage. They, together with their four oxygen neighbors, form *cage poles* [see Fig. 1(b)]. The five atoms of each pole are located almost in one plane with the sum of O-Ca-O angles, as calculated for an empty cage, amounting to 358°, i.e., the Ca(I) ions are exposed to the negative charge density due to an extraframework species. Four other Ca ions, Ca(II), all Al, and the remaining O ions form the *cage belt*. Cations of the cage belt are effectively "screened" by the cage-wall oxygen ions from the effect of the charge density of the extraframework species. A line drawn between two Ca(I) ions passes through the center of the cage and corresponds to the S_4 symmetry axis. The S_4 symmetry is preserved only approximately because the cages are distorted by the extraframework ions.

B. Experimental data

Our theoretical work was motivated by a series of recent publications where properties of hydrogenous species in C12A7 were studied experimentally.[4,14–18] In the following we briefly describe the results of some of these experiments.

It was noted that if the C12A7 is heated to temperatures between 800 and 1300 °C in a hydrogen-containing atmosphere and then quenched rapidly to room temperature, the relative concentration of different hydrogenous species in the C12A7 changes so that the sample becomes optically active as described below. We will refer to this procedure as H treatment and C12A7:H will denote the H-treated C12A7.

The total content of hydrogenous species was determined using the secondary ion mass spectroscopy technique.[4] Then, with the help of infrared (ir) spectroscopy, it was possible to make a quantitative estimate of the number of OH^- ions present in the C12A7 samples before and after such treatment. To establish which other species were present in C12A7:H, a careful search for paramagnetic species such as H^0, H^{2-}, and H_2^- as well as for diamagnetic H_2 and H_2O molecules was undertaken using electronic paramagnetic resonance (EPR) and ir spectroscopies. The results demonstrated that the concentration of these defects was below the detection levels of 10^{16} and 10^{18} cm^{-3} for the EPR and ir measurements, respectively. On the basis of this analysis a concentration in the order of 10^{20} cm^{-3} was assigned to H^- species, which are EPR "silent" and can hardly be detected with ir or Raman spectroscopies. It has to be stressed that while this analysis allows one to determine relative concentrations of hydrogenous species in H-treated C12A7, it gives no information on their content *during* the H-treatment procedure.

The exact mechanism of hydrogen doping of C12A7 is not known (see also Sec. IV A below). However it was established that the doping is not confined to the near-surface layer but permeates the whole bulk of the sample. It is therefore reasonable to suggest that the extraframework species O^{2-}, OH^-, and H^- are distributed homogeneously in C12A7:H so that there are no regions of excessive net lattice charge, either positive or negative, or measurable density fluctuations of hydrogenous species.

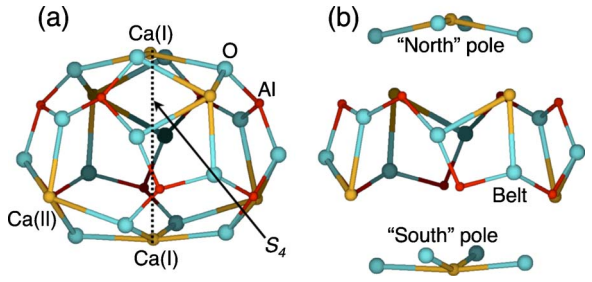

FIG. 1. (Color online) (a) A single empty cage of the C12A7 framework as relaxed using the embedded cluster approach. The cage wall includes six Ca ions shown in yellow (small light gray), eight Al shown in red (small dark gray), and 16 O ions shown in blue (large light gray). The dashed line indicates the S_4 symmetry axis of the cage. The two Ca ions at the poles of the cage are shown as Ca(I), while Ca(II) indicates cage-belt Ca. (b) Atoms of the cage poles and those of the cage belt.

The C12A7:H samples were then irradiated with uv light at room temperature. As a result the originally insulating and transparent C12A7:H became an electronic conductor and acquired a greenish color while remaining transparent (over 95% transmission in the visible light range is preserved for 200-nm-thick films). These changes were induced by photons in the energy range 3.5–5 eV with the largest coloration sensitivity observed at 4.1 eV.[4] The insulator-conductor transition was also accompanied by the formation of two optical absorption bands with maxima at approximately 0.4 and 2.8 eV as well as by the appearance of a strong EPR feature due to an unpaired electron spin. The magnitude of these changes is almost proportional to the estimated concentration of H^- species in C12A7:H and to the intensity of the irradiation.

Further study of the temperature dependence of the photoinduced processes in C12A7:H revealed[18] that the coloration efficiency at room temperature is higher than at temperatures below 100 K. The EPR measurements of samples irradiated at 4.2 K show that not only unpaired electrons but also H^0 atoms are present in the system. On the contrary, samples irradiated at room temperature and then cooled down to 4.2 K for EPR measurements showed no signs of H^0 with only the unpaired electrons being present. The thermal stability of H^0 atoms was investigated using the isochronal annealing technique. It was shown that as annealing temperature increases, the concentrations of both unpaired electrons and H^0 atoms decrease until approximately 100 K where the concentration of H^0 atoms falls below the detection limit and that of the electrons plateaus and remains constant up until 300 K.

While the coexistence of transparency and high electrical conductivity has been previously explored theoretically by us in Refs. 5 and 6, the mechanisms of the transformation from the insulating to the conductive state in C12A7:H were only briefly addressed.[13,19,20] We discuss detailed processes involved in such transformation in this study.

III. DETAILS OF THE CALCULATIONS

Three computational methods were used in this work. First, the dynamics of H_2 molecules in the C12A7 bulk was investigated using the quantum-mechanical molecular dynamics (QMMD) approach as described in Sec. III A. The results of the QMMD simulations were used in the modeling of the interaction of H_2 molecules with the C12A7 lattice using the embedded cluster approach (see Sec. III B). The same embedded cluster approach was applied to study the mechanisms of photoionization of H^- species in C12A7:H and to consider mechanisms for the subsequent recombination and defect-formation processes. Finally, to support the results of the embedded cluster calculations we considered the electronic structure of the extraframework electrons in C12A7 using the periodic model and a density functional approach as described in Sec. III C.

A. Parameters of periodic plane-wave density functional theory calculations

The behavior of a H_2 molecule in the C12A7 lattice was studied using a so-called quantum-mechanical molecular dynamics approach in which the motion of atoms is described using classical Newtonian equations, while the total energy of the system and forces acting on atoms are calculated quantum mechanically. The simulations were carried out at 1600 K, which is close to the experimental conditions used in the H-treatment procedure.[4] We employed the periodic model and the VASP code,[21] which implements the density functional approach in the generalized gradient approximation of Perdew and Wang[22] and uses a plane-wave basis set. The spin-unpolarized mode was used in these calculations. The core electrons were represented using projected augmented-wave pseudopotentials,[23,24] which provide electronic configurations $[Ne]3s^23p^64s^2$ for Ca, $[Ne]3s^23p^1$ for Al, and $[He]2s^22p^4$ for O atoms. The C12A7 was represented using a 118-atom cubic unit cell which includes 116 framework atoms and two extraframework O^{2-} ions located in two randomly selected cages. Such a configuration reflects a disordered arrangement of the extraframework O^{2-}, which are very mobile at high temperatures.[25,68] An energy cutoff of 500 eV and a single k point (Γ) in the reciprocal space were used in these calculations. Prior to the QMMD calculations, the total energy of the system was minimized with respect to both fractional coordinates and the size of the cubic unit cell. The optimized lattice constant of 12.07 Å is only 0.7% larger than the experimental value of 11.99 Å.

B. Embedded cluster method

The properties of hydrogenous species in C12A7 under irradiation with uv light were studied using an embedded cluster technique,[5,26] which allows one to calculate the optical, paramagnetic, and transport properties of individual defects. In this method, a cluster with a defect considered quantum mechanically is embedded in the rest of the polarizable crystal considered classically using the shell model.[27] This allows one to account for the defect-induced lattice polarization and to incorporate the effect of this polarization on the defect properties. This technique has been thoroughly described in Refs. 5, 26, and 28 and tested in defect studies of several oxides.[5,29–31]

The C12A7 crystal is represented by a large finite nanocluster of nearly spherical shape built from 64 unit cells and divided into regions I and II. A quantum-mechanically considered cluster (QM cluster) built of two adjacent cages (two-cage cluster hereafter) is placed at the center of the nanocluster and is surrounded by a spherical region I with a radius of about 13 Å, in which the polarizable lattice is represented atomistically. The remaining part of the nanocluster, region II, is also considered atomistically but in the nonpolarizable lattice approximation. Ions outside the QM cluster are treated using a classical model and interatomic potentials with a rigid atom approximation. The rigid atom parameters were obtained from the original set of interatomic potentials developed for the shell model calculations of Al or Fe disorder in $Ca_2Fe_xAl_{2-x}O_5$ compounds.[32] In particular, we used the same parameters of the interatomic potentials but removed the shells from oxygen ions. As a result of such modification the calculated unit cell volume changed by 0.5% and the elastic constants changed on average by 4.7%. All centers

in region I, containing about 700 atoms, are fully relaxed in the course of energy minimization while those in the rest of the nanocluster are kept fixed in perfect lattice positions. An interface between the QM cluster and classical ions is introduced to prevent an artificial spreading of electronic states outside the QM cluster. Ca and Al ions in the interface region are represented using "large-core" LANL1 effective core pseudopotentials (ECPs) and interact quantum-mechanically with atoms of the QM cluster and classically with the classical environment.

The embedded cluster technique discussed above is implemented in the computer code GUESS (Gaussians used for embedded system studies), which interfaces the GAUSSIAN98 package[33] for quantum-mechanical calculations with a program for classical calculations using the shell model available within the GUESS code. Calculations were made using density functional theory with a hybrid density functional B3LYP. This functional combines Becke's three-parameter hybrid exchange functional[34] with the correlation functional by Lee, Yang, and Parr.[35] One of the important advantages of using this functional is that it reproduces the band gaps of insulators with good accuracy.[36] The optical transition energies were calculated using the time-dependent density functional theory (TDDFT) method as implemented in the GAUSSIAN98 package. All oxygen ions were considered using the standard all-electron 6-31G basis set, while Ca and Al ions used the "small-core" LANL2 effective core pseudopotential and the LANL2DZ basis set.[37,38] Finally we note that the embedded two-cage QM cluster is sufficient to model accurately the diffusion, reaction mechanisms, and photoexcitations considered in this work. Processes involving simultaneous changes of the electronic structure of species located in three or more cages are not considered here.

C. Parameters of periodic atomic-basis hybrid DFT calculations

The electronic structure of C12A7 containing extraframework electrons was also calculated using the hybrid B3LYP density functional and the periodic model. A Gaussian-type atomic basis set and the CRYSTAL03 computer code[39] were used. Similarly to the case of plane-wave DFT calculations, a single k point (Γ) in the reciprocal space was considered in these calculations. The initial configuration of C12A7 extraframework species included two O^{2-} ions; it was then modified to include extraframework electrons (see the Appendix). Use of diffuse Gaussian-type functions, e.g., those representing valence electronic shells of Ca and Al atoms, meets certain computational difficulties in calculations of the exchange interaction in the periodic model. Therefore, we could not employ here the basis set that was used in the embedded cluster approach. Instead, basis sets were taken from the CRYSTAL basis set database;[40] 86-511G and 8-511G basis sets for Ca and Al were optimized for CaO and Al_2O_3, respectively; the 8-411G basis set for oxygen, as generally recommended for studies of ionic oxides, was used. In addition, a single *sp* Gaussian function was positioned at the center of each empty cage. This is necessary to provide sufficient variational freedom for the electron density to be distributed over the empty volume of the cages as well as over the framework. The exponential factor of this function, 0.217 $Bohr^{-2}$, was taken as an arithmetic average over the exponential factors of the most diffuse functions of the Ca, Al, and O basis sets.

IV. RESULTS OF THE CALCULATIONS

A. Mechanisms of H^- formation in C12A7

Exposure of C12A7 to H_2 gas at high temperatures increases the content of hydrogenous species in C12A7 bulk as well as changes their relative concentrations as discussed in Sec. II B. Understanding of the H-incorporation mechanisms is essential for identification of the types of hydrogenous species formed in this process. It is difficult to obtain experimental information on the details of H incorporation. Therefore development of theoretical models is of great use.

Incorporation of C12A7 with hydrogen may take place via several channels. These can be divided into two groups. The first group of mechanisms involves adsorption of an H_2 molecule from the gas phase onto C12A7 surface with consequent dissociation into a pair of either H^0 atoms or H^+ and H^- ions. These process are known to take place, for example, at the surfaces of ionic compounds such as MgO.[41–43] The H atoms or ions can then diffuse into the C12A7 bulk along their respective diffusion gradients. Another group of mechanisms involves diffusion of H_2 molecules into C12A7 bulk where they participate in chemical reactions with bulk C12A7 species. The in-diffusion of H_2 molecules is known to take place in materials with open lattices such as silica[44] and zeolites.[45,46]

Since there is no solid experimental data, that could help to differentiate reliably between the two types of doping mechanisms, we assume, by analogy with other nanoporous materials, that in-diffusion of H_2 molecules can take place in C12A7. This mechanism serves as a modeling tool to find the most stable hydrogenous species at the thermal equilibrium. The final products of H incorporation should not depend on the path chosen. The interaction of H_2 molecules with C12A7 lattice species and energetics of several possible reaction mechanisms will be considered in the remaining part of this section.

First we simulated the behavior of a H_2 molecule in C12A7 at the conditions used in the H-treatment procedure. The dynamics of a H_2 molecule were studied using the periodic plane-wave DFT and QMMD technique as described in Sec. III A. A unit cell containing two extraframework O^{2-} ions was considered and a single H_2 molecule was positioned in an empty cage. The system was first fully relaxed in a static energy minimization calculation. The H_2 molecule in the equilibrium configuration occupies a site in the middle of the cage and its molecular axis is oriented approximately perpendicular to the S_4 symmetry axis of the cage with a H-H distance of 0.764 Å. The dynamics of the system were monitored at 1600 K for 3 ps.

Analysis of the temperature-induced motion of the H_2 molecule shows that the molecule exhibits stretching vibrations; it also rotates freely within the cage and occasionally collides with the cage wall. The collision events can be clas-

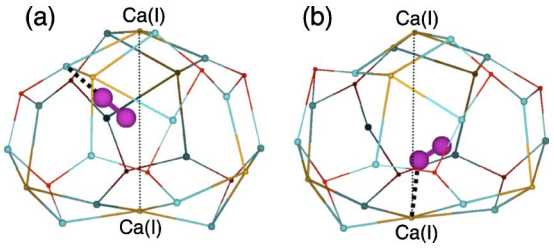

FIG. 2. (Color online) Two QMMD snapshots showing typical configurations of "dissociation attempts" found for H_2 molecules in C12A7: (a) H_2 interacts with a cage-wall oxygen ion, (b) H_2 interacts with one of the Ca(I) ions at the cage poles. Atoms notations are as follows: Ca, yellow (small light gray); Al, red (small dark gray); O, blue (large light gray); H, purple (large dark gray). The thick dotted lines point to the nearest cage wall ions while the thin dotted lines indicate the cage S_4 axes. The cages are distorted due to thermal fluctuations.

sified into two types as shown in Figs. 2(a) and 2(b), respectively, which are, effectively, "mirror images" of each other. In a collision of the first type [Fig. 2(a)] a H atom bounces into a cage-wall oxygen; the H_2 molecule is oriented so that the other H atom is approximately halfway between the two Ca(I) atoms at the cage poles. In the event of such collisions the interatomic distance in the H_2 molecule increased to 0.87–0.92 Å as compared to the average H-H distance of 0.792 Å found at 1600 K. In collisions of the second type [see Fig. 2(b)] one of the H atoms approaches one of the Ca(I) atoms at a cage pole with the H_2 molecule oriented so that the other H atom points toward one of the cage wall oxygens.

Similar configurations of an H_2 molecule at oxide surfaces (see, for example, Ref. 42 have indicated possible dissociation channels into H^+ and H^- species. Although the dissociation process itself was not observed on the time scale of our QMMD simulation, these results provide valuable clues for understanding the behavior of H_2 at high temperature.

The encaged H_2 molecule was then considered using the embedded cluster approach. Static energy minimization calculations reveal that the potential energy surface of H_2 has an energy minimum in the middle of a cage. The configuration of H_2 is very similar to that found in the periodic plane-wave DFT calculations; the H-H distance in this case is 0.763 Å. This, however, is not a thermodynamically stable configuration as we discuss below.

We then calculated the electronic structure of the system using the geometrical configurations that correspond to the collision types described above. It was found that the H_2 molecule in these configurations becomes strongly polarized, i.e., it adopts a H^{q-}-H^{q+} electronic configuration, with the negatively charged H being between the two Ca(I) atoms at the cage poles and the positively charged H oriented toward a cage-wall oxygen ion. We have then explored the possibility of the dissociation of H_2 into a pair of H^- and H^+ ions (H^+/H^- configuration thereafter). One of the hydrogen atoms of the H_2 molecule was displaced toward a cage wall O^{2-} and fixed, while *all* other atoms in region I were fully relaxed. Geometry configurations found for several such displacements determine the dissociation pathway. The total energies of the molecular H_2 and dissociated H^+/H^- configurations were almost identical and the calculated energy barrier between the corresponding potential wells was just over 0.2 eV. In the dissociated configuration the H^- ion occupies a site almost exactly at the center of the cage, while the proton "sticks" to the cage wall and forms an OH^- ion there. This OH^- ion is oriented so that the proton is pointing toward the H^- at the cage center and the distance between them is 1.47 Å.

Taking into account the small energy barrier separating the H_2 and H^+/H^- configurations described above, they should coexist at high temperatures. Both configurations are metastable and can be transformed further. The thermodynamically most stable configuration we have found is obtained via the reaction of an H_2 molecule with an extraframework O^{2-} (as opposed to a cage-wall O^{2-}) with formation of an extraframework OH^- and H^-. The calculated activation energy of H_2 diffusion required for this process is about 2.2 eV. As soon as the H_2 reaches an intercage opening between an empty cage and a cage occupied by an extraframework O^{2-}, it splits so that OH^- and H^- are formed in neighboring cages. The reaction is highly exothermic with a total energy gain of about 2.2 eV. The same thermodynamical state can be obtained from a H^+/H^- configuration described above. In this case the proton diffuses through the lattice with an activation energy of 1–1.5 eV and reacts with an extraframework O^{2-}.

We have also considered the possibility of the homolytic dissociation of H_2 into a pair of H^0 atoms. Since the QMMD calculations were carried out using spin-restricted DFT, a possible channel for homolytic dissociation of H_2 into a pair of H^0 atoms was suppressed. This, however, does not affect the results of this section since the energy required to break H_2 into a pair of atoms is about 4.7 eV in our calculations. This energy cannot be compensated by the energy gain due to the interaction of H^0 atoms with the cage-wall ions (approximately 0.3 eV).

Nevertheless, a homolytic dissociation of H_2 can be induced if the H_2 interacts with an extraframework O^- ion. The products of this reaction are an extraframework OH^- and a hydrogen atom while the energy gain is about 0.35 eV. The thermal stability of H^0 atoms is considered below in Sec. IV D. This reaction channel, however, is heavily suppressed with respect to those described above because extraframework O^- ions are never the dominant species in C12A7. We would like to note that the interactions of H_2 with both O^{2-} and O^- find their analogies in the behavior of H_2 molecules at MgO surfaces.[41–43] We discuss this analogy in more detail in Sec. VI.

Thus we conclude that H_2 molecules incorporated in the C12A7 lattice can participate in several chemical reactions with both framework and extraframework O^{2-} ions and result in the formation of extraframework H^- species in the middle of a corresponding C12A7 cage. These species will be referred to as encaged or interstitial H^- ions. H^+ species, also formed in these reactions, are effectively trapped by the extraframework O^{2-} ions and do not take place in further transformations. We stress that direct experimental observation of interstitial H^- species has not yet been carried out. Therefore theoretical validation of its formation is a necessary step in our modeling.

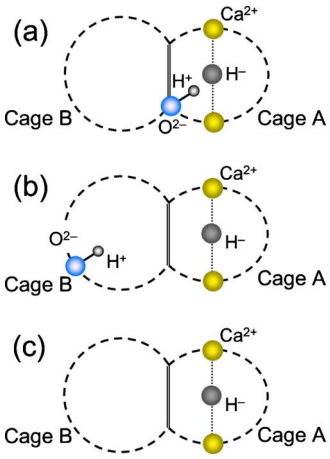

FIG. 3. (Color online) Configurations of H^+ and H^- ions considered in the calculations of photoinduced ionization of H^- species: (a) dissociated but not separated pair, (b) H^+ and H^- ions separated in neighboring cages, and (c) infinitely separated pair. The cage walls are shown schematically with dashed lines. Thin dotted line in cage *A* shows the S_4 symmetry axis connecting two Ca(I) ions at the cage poles. The types of atoms and their formal charge states are shown explicitly. The effect of the H^- on the relaxation of the cage wall is indicated with smaller cage size.

B. Photoionization of H^- ions

To study the interaction of encaged H^- ions with uv light we have calculated their optical absorption using TDDFT. Since H^- species are formed as a result of H_2 dissociation into H^- and H^+ (the latter appears in the form of OH^- ion) as discussed in Sec. IV A, the optical absorption of H^- species will depend on the distance between H^- and H^+. Therefore, the excitation energies and the nature of singlet→singlet transitions were calculated for several geometrical configurations of H^- shown in Fig. 3. The configuration of dissociated but not separated H^+ and H^- ions is shown in Fig. 3(a), where both ions occupy the same cage, while the neighboring cage remains unoccupied. A configuration representing a case of intermediate separation between H^+ and H^-, which could be achieved, for example, via H^+ diffusion, is shown in Fig. 3(b). Here the H^+ and H^- ions occupy two neighboring cages. Finally, a case of a fully separated pair is shown in Fig. 3(c), where only an H^- ion is present.

The 15 lowest excited states were calculated for each configuration. We found that in all cases the lowest-energy excitation corresponds to an electron transfer from H^- in cage *A* to the neighboring cage, cage *B*, so that the excited state is characterized by separated H^0 atom and e^-. This configuration is referred to as $[H^0]_A[e^-]_B$ or $[H^0][e^-]$ for brevity. The isosurface for the molecular orbitals of H^- and of an empty cage, as calculated for configuration $[H^-][\text{null}]$, are shown in Figs. 4(a) and 4(b), respectively. The presence of the H^+ ion in configurations $[H^+/H^-][\text{null}]$ and $[H^-][H^+]$ perturbs these orbitals but does not change the nature of the transition.

The optical absorption energies calculated for all three configurations are summarized in Table I. It is clearly seen that the excitation energies of H^- are affected by the relative position of the proton. For example, if the proton is in the same cage as H^-, it deepens the potential well for the H^- electrons and, therefore, results in a larger excitation energy. On the contrary, if H^+ occupies an empty cage, it deepens the potential well for the excited electron and the excitation energy becomes smaller. The calculated oscillator strengths for these transitions are close to 0.01; these relatively small values are due to the small overlap of the localized orbital of the H^- and that of the empty cage.

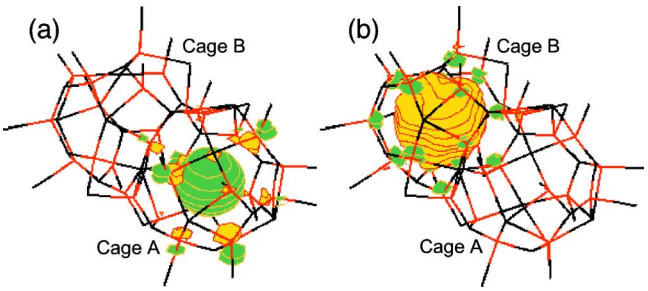

FIG. 4. (Color online) Molecular orbitals calculated for $[H^-][\text{null}]$ configuration: (a) highest occupied orbital describing two electrons of H^- ion in cage *A*; (b) lowest unoccupied orbital describing the unoccupied state in the empty cage *B*. Thin red (gray) and black lines connect the neighboring atoms of the QM cluster.

We therefore conclude that exposure of H^- containing C12A7 to 3.8–4.5 eV photons will result in photoionization of the H^- ions leading to the formation of localized extra-framework electrons and H^0 atoms ($[H^0][e^-]$). This agrees well with the experimentally observed coloration of C12A7:H under irradiation with 3.5–5 eV photons as discussed in Sec. II B.

Second and higher excited states calculated for these configurations correspond to the transitions from the top of the valence band (VB) to the lowest unoccupied *s*-like state in cage *B* shown in Fig. 4(b). Such unoccupied states form the so-called *cage conduction band* (CCB) as we discussed earlier[5,6,19] (see also the Appendix below). The calculated excitation energies for VB→CCB optical transitions are 5.2 eV and higher. This agrees well with the optical absorption edge measured for intrinsic C12A7 crystals at about 5 eV.[4] Thus, the significant redshift to approximately 4 eV observed[4] for C12A7:H is reproduced well in our calculations.

The nature and energetics of optical transitions of C12A7:H can be compared to those reported earlier in Ref. 13. This work suggests that a transition from the 1*s* state of H^- to the 3*d* states of neighboring Ca atoms can be excited at

TABLE I. Excitation energies for several configurations of encaged H^- ions. The energies are given in eV; the oscillator strengths are calculated using the dipole moment operator.

	Configuration		Excitation	
N	Cage *A*	Cage *B*	Energy	Oscillator strength
i	H^-/H^+	Null	4.5	0.0068
ii	H^-	H^+	3.8	0.0076
iii	H^-	Null	4.3	0.0091

5.2 eV. This energy is about 1 eV higher than that both observed experimentally and found in our calculations. Moreover, the nature of the transition is also different from that found in the present work. Such disagreement can be attributed to primarily three factors. First, the calculations reported in Ref. 13 do not show the cage conduction band formed by the states associated with empty cages. These states, however, are shown to exist in our calculations[5,6,19] and also in independent plane-wave DFT calculations by Li *et al.*[47] Second, the significant lattice relaxation induced by the charged species was neglected in Ref. 13. Finally, the excitation energies reported in Ref. 13 were calculated from the DFT density of one-electron states, while we are using the TDDFT approach.

C. Extraframework electrons in C12A7 lattice

The results of our earlier embedded cluster calculations suggest that the extraframework electrons in C12A7 induce a strong lattice relaxation, which results in trapping and localization of the extraframework electron in an empty cage.[5,6] The most prominent feature of this relaxation is the displacement of the two Ca(I) atoms at the poles of an empty cage toward the cage center. This property of the extraframework electrons results in their effective spatial separation from the H^0 atoms and plays an important role in suppressing the $H^0+e^- \rightarrow H^-$ recombination, as discussed in the next section.

To make sure that the localization of the extraframework electrons in empty cages is not an artcfact of the embedded cluster approach we carried out a series of periodic model calculations for different concentrations of the extraframework electrons. The CRYSTAL03 code and the B3LYP functional were used in these calculations (see Sec. III C). There are two factors that governed the choice of the method. First, it is known that the exact exchange contribution to the density functional is needed to reproduce polaron states in DFT calculations (see, for example, Refs. 48–50 and references therein). Moreover, the calculated band gap strongly depends on the amount of the exact exchange used in the calculations.[51] The band gaps calculated using the hybrid B3LYP density functional used in CRYSTAL calculations are in generally good agreement with the experimental data.[36] Second, the aim of the current calculations was to compare the periodic and the embedded cluster approaches. Therefore we used similar basis sets and methods in both cases.

The results of the periodic model calculations are summarized in the Appendix. In brief, we find that at low concentrations (one e^- per cubic unit cell) the extraframework electrons are well localized in a single cage. The band structures plotted in Fig. 7 in the Appendix show that the extraframework electron state has almost no dispersion. The spin density calculated for this system plotted in Fig. 8 shows a single peak in the middle of a cage. At high concentrations the extraframework electrons become less localized as indicated by the dispersion of the corresponding states (see Fig. 9). Thus, both the periodic and embedded cluster calculations give a consistent set of results and support the localized polaron nature of extraframework electrons. Finally we note that the localization of electrons can take place not only in crystalline materials but also in other media as has been demonstrated for solvated electrons (see, for example, Refs. 52 and 53).

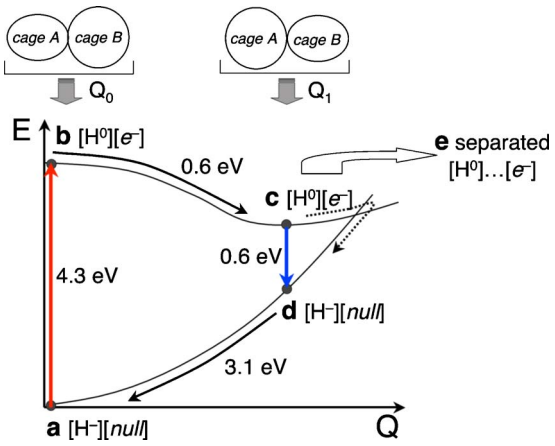

FIG. 5. (Color online) Processes induced by the photoionization of encaged H^-. *a-b*, Frank-Condon transition $S_0(Q_0) \rightarrow S_1(Q_0)$, which corresponds to the photoexcitation $[H^-][\text{null}] \rightarrow [H^0][e^-]$. *b-c*, Relaxation of the excited state S_1: $S_1(Q_0) \rightarrow S_1(Q_1)$. *c-d*, Radiative $S_1(Q_1) \rightarrow S_0(Q_1)$ (solid line) and nonradiative (dotted line) transition deexcitation. *c-e*, Thermally activated separation of H^0 and e^-. *d-a*, Relaxation to the ground state configuration: $S_0(Q_1) \rightarrow S_0(Q_0)$. Thin lines *b-c* and *d-a* are shown only to guide the eye.

D. Transformation of the H^0+e^- electronic configuration

The excited state configuration $[H^0][e^-]$ [see Fig. 5(b)] considered above can transform via several channels that can be loosely divided into *recombination* and *separation* channels. The latter can be stabilized via thermally activated *annihilation* of H^0 atoms. Both types of mechanisms are described below.

1. Recombination and separation channels

To investigate the recombination channel we considered the $[H^-][\text{null}]$ configuration discussed previously in Sec. IV B. The ground state of this system is defined as S_0 and the corresponding total energy as E_{S_0}. The equilibrium lattice geometry obtained for this configuration is defined as Q_0 in Fig. 5. The lowest singlet→singlet transition which induces ionization of H^- was calculated using the TDDFT approach as described in Sec. IV B and the total energy of this excited state is defined as E_{S_1}. The character of the transition and the corresponding excitation energy (see also Table I) are shown in Fig. 5.

Point *c* in Fig. 5 indicates the relaxed excited state S_1 and the corresponding lattice geometry Q_1.[54] As a result of the $S_1(Q_0) \rightarrow S_1(Q_1)$ relaxation (indicated by path *b-c* in Fig. 5) the cage containing the excited electron (cage *B*) contracted and the distance between Ca(I) for this cage decreased from 5.46 to 5.01 Å. At the same time, cage *A* expanded and the corresponding Ca(I)-Ca(I) distance increased from 4.97 to 5.53 Å. Such a relaxation represents the reaction of the C12A7 lattice to the transfer of a single electron charge from one trapping site to another.

To find the $S_1(Q_0) \rightarrow S_1(Q_1)$ relaxation energy and the energy of the radiative deexcitation $S_1(Q_1) \rightarrow S_0(Q_1)$ (path *c*-*d* in Fig. 5) we first calculated the total energy of the singlet ground state for geometry Q_1, $E_{S_0}(Q_1)$, shown as point *d* in Fig. 5. Then the energy of the lowest excited singlet state $E_{S_1}(Q_1)$ shown as point *c* in Fig. 5 was calculated using the TDDFT approach. The relatively small energy gain in the $S_1(Q_1) \rightarrow S_0(Q_1)$ transition indicates that these states cross over not far from the energy minimum of the state S_1. Therefore, the nonradiative transition *c*-*d*, indicated with the dotted line in Fig. 5, is expected to significantly quench the radiative transition *c*-*d*.

The diagram in Fig. 5 shows a possible pathway for the recombination of the H^0 and e^- pair in the neighboring cages and the energies associated with this pathway. The H^0 atom and the excited e^- are already separated in the configuration shown at *c* in Fig. 5. We can consider the state $S_1(Q_1)$ at *c* in Fig. 5 as a branching configuration between the $H^0 + e^- \rightarrow H^-$ recombination on one hand and further separation of H^0 and e^- on the other. To suppress the recombination the system has to progress to a state where the electron is separated further from the H^0 atom. Such separation can be achieved if either one or both of these species are mobile. As we have shown previously,[5,6] the extraframework electrons at low concentrations move via thermally activated hopping with an activation energy close to 0.1 eV. Thus the probability of separation of these two species increases with temperature, which is consistent with the experimentally observed increase in the coloration efficiency with increasing temperature.

2. Annihilation of H^0 atoms

We can distinguish three possible mechanisms of thermally activated annihilation of H^0 atoms. The first one involves two hydrogen atoms that appear in the neighboring cages as shown in Fig. 6(a). This situation can be realized at high levels of H doping, under intense uv irradiation and high temperature which, in turn, facilitates high H^0 mobility. The charge transfer of an electron from one H atom to another, accompanied by lattice relaxation, results in the formation of the $[H^+][H^-]$ configuration. The energy gain in this process, as calculated using the unrestricted DFT approach and B3LYP density functional, is 3.5 eV. We note that $[H^0][H^0] \rightarrow [H^+][H^-]$ relaxation itself is not thermally activated and happens spontaneously.

The second transformation channel involves the diffusion of a H^0 atom through the C12A7 lattice and its reaction with an extraframework O^{2-} ion. This reaction results in the formation of a OH^- ion in the middle of a cage and an extraframework electron as indicated in Fig. 6(b). The energy gain in this process is close to 2.5 eV. The calculated activation energy for this H^0 diffusion is approximately 0.6 eV. This is in line with recent experimental and theoretical studies of H^0 diffusion in, for example, SiO_2, which indicate that the H^0 diffusion activation energy can be between 0.1 and 0.4 eV.[55,56]

The "mean free path" of H^0, i.e., the distance it travels before it reacts with an extraframework O^{2-} ion, can be easily estimated. Since O^{2-} ions are the dominant extraframework species in the C12A7 lattice, we can assume that their concentration is close to that in stoichiometric C12A7, i.e., one in six cages contains an extraframework O^{2-}. This is the equivalent of having 1.5 cages occupied by O^{2-} ions and 7.5 empty cages for each nine cages of the framework. Let us define the cage-to-cage transfer of an H^0 atom as a single diffusion step. Then the probability of H^0 diffusion into an empty cage at the first diffusion step is 7.5/9. At the second and following diffusion steps the probability of diffusion into an empty cage is 6.5/8 because the "return" to the cage occupied at the previous step should not be included in the calculation. Thus the probability of H^0 *not* interacting with extraframework O^{2-} after *n* steps is $(7.5/9)(6.5/8)^{(n-1)}$. Since the distance between the cage centers is about 6 Å, the mean free path for H^0 atom diffusion is less than 27 Å.

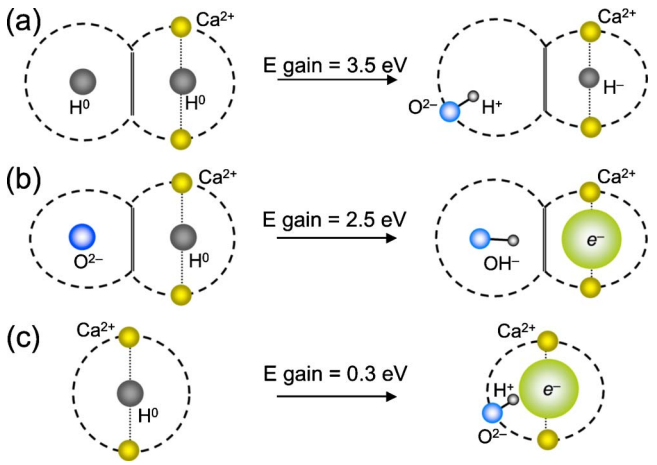

FIG. 6. (Color online) Possible mechanisms of thermally activated decay of H^0 atoms in C12A7: (a) spontaneous charge transfer accompanied by the lattice relaxation, (b) diffusion of H^0 through the C12A7 lattice and reaction with an extraframework O^{2-} ion, and (c) reaction of H^0 with a cage-wall O^{2-} ion. Positive energy gains suggest that there are at least three mechanisms that result in the decrease of H^0 atom concentration. The cage walls are shown schematically with the dashed lines. Atom types and their charge states are shown explicitly.

Finally, an H^0 atom can also react with an O^{2-} ion in the cage wall and form a cage-wall OH^- and an extraframework electron as shown in Fig. 6(c). The energy gain in this process is only 0.3 eV. Since the energy gain in this case is much smaller than in the processes shown in Figs. 6(a) and 6(b), this configuration is not thermodynamically stable. We have considered two possible routes of further relaxation. One of them involves the diffusion of the proton through the lattice, with a calculated activation energy of ca. 1–1.5 eV, followed by its reaction with an extraframework O^{2-}. The energy gain in this second leg is 2.2 eV and the final state is the same as that shown in Fig. 6(b).

Another possible mechanism involves the recombination of the proton and the extraframework electron with formation of an H^0 atom [i.e., the process opposite to that shown in Fig. 6(c)] followed by the diffusion of the H^0 atom through the C12A7 lattice and its reaction with an extraframework O^{2-}, as shown in Fig. 6(b). We note that the species involved

in both reactions $H^+ + O^{2-} \rightarrow OH^-$ and $H^0 + O^{2-} \rightarrow OH^- + e^-$ have comparable diffusion activation energies (the experimental estimate[10] for the O^{2-} activation energy is 0.82 eV). However, the diffusion of H is expected to be more rapid than that of O due to the significant difference in their masses.

We conclude, on the basis of the results presented in this section, that H^0 atoms formed as a result of photoionization of H^- are transient species. Their concentration decreases both via recombination with extraframework electrons and via chemical reactions with extraframework O^{2-} ions.

V. SUMMARY OF THE MODEL AND COMPARISON WITH THE EXPERIMENTAL DATA

The results described in Sec. IV allow us to build a consistent physical picture of the photoinduced processes in C12A7:H and compare them with available experimental data.

The exposure of "as-grown" C12A7 to H_2 gas at high temperatures results in the modification of the extraframework species. In particular, some of the extraframework O^{2-} ions can be transformed into a pair of H^- and OH^- located in different cages as described in Sec. IV A.

Subsequent irradiation of this system with photons of 3.8–4.5 eV results in the photoionization of H^- species and the formation of H^0 atoms and extraframework electrons which then localize in empty cages (see Sec. IV B). The extraframework electrons induce an intracage optical absorption band at 2.8 eV, which is responsible for the greenish color of irradiated C12A7 samples.[5,6] They also exhibit polaron behavior by hopping from one empty cage to another with an estimated activation energy of about 0.1 eV.[5,6] These theoretical findings are consistent with the experimentally observed coloration and electrical conductivity induced by uv irradiation of C12A7:H with 3.5–5 eV photons. The experimental maximum of the sensitivity of C12A7:H to UV light was found at 4.1 eV.[4]

The system containing both H^0 atoms and extraframework electrons is in a metastable state as discussed in Sec. IV D. If the mobility of H^0 and e^- is low and they remain in neighboring cages, they can recombine and form H^-. This is consistent with the low coloration efficiency observed at temperatures below 100 K. At higher temperatures, as the mobility of both e^- and H^0 increases, they can become separated. Then, the H^0 can diffuse through the C12A7 lattice and react with an extraframework O^{2-} ion forming an OH^- ion and another extraframework electron (see Sec. IV D). This process suppresses the recombination channel of H^0 and e^- and increases the coloration efficiency (see Sec. II B). The theoretical prediction of thermally activated decay of H^0 atoms is in agreement with the experimental fact that H^0 atoms are observed only if C12A7:H was irradiated at temperatures below 100 K.

Thus, the long-term stability of the extraframework electrons in postirradiation C12A7:H samples is explained by the suppression of the $H^0 + e^- \rightarrow H^-$ recombination channel. It follows from our results that the maximum concentration of *thermally stable* extraframework electrons in C12A7:H could be achieved if the preirradiated sample has the chemical composition $[Ca_{24}Al_{28}O_{64}] \cdot O^{2-} OH^- H^-$, which becomes $[Ca_{24}Al_{28}O_{64}] \cdot 2OH^- 2e^-$ after irradiation and subsequent relaxation. Moreover, samples with eight extraframework electrons per cubic unit cell could be formed if the preirradiated samples were $[Ca_{24}Al_{28}O_{64}] \cdot 4H^-$. In this case the processes described above may result in a $[Ca_{24}Al_{28}O_{64}] \cdot 4H^+ 8e^-$ configuration where all the extraframework protons are attached to cage-wall oxygens. This, however, is likely to be only a metastable state with a small barrier for the recombination process.

The model presented above also explains why electrical conductivity and the change in color of uv-irradiated C12A7:H samples are observed only in the irradiated area. These changes, as described in our earlier work,[5,6] are induced by the extraframework electrons. Given that the extraframework anions (O^{2-}, OH^-, H^-) in preirradiated C12A7:H are distributed homogeneously so as to compensate the positive charge of the framework, the uv irradiation converts one type of negative extraframework species (H^-) into another (e^-). The electrons, however, cannot leave the irradiated area because this would create regions with net positive charge, which would not be compensated by the significantly less mobile extraframework O^{2-}, OH^-, and the remaining H^- species.[4,25,57,58] The H^0 atoms also formed after the photoionization of H^- ions are neutral and have a relatively low diffusion activation energy (see Sec. IV D). They will also contribute to the formation of stable and extra-framework electrons according to the reaction shown in Fig. 6(b). However, the mean free path of these H^0 atoms is less than 3 nm because the significant number of extraframework O^{2-} ions in the system (approximately 10^{21} cm^{-3} under the conditions of the experiment[4]) serve as traps for H^0 atoms. We can therefore predict that the uv-induced conductivity and color change would spread outside the irradiated area only if the concentration of H^0 traps, such as O^{2-} and O^- species, is significantly reduced.

The mechanisms of photo-induced conductivity in uv-irradiated C12A7:H have recently been addressed in Refs. 13 and 20. We would like to highlight the important differences between the models presented there and in this work. While there is a consensus that the conduction electrons in C12A7:H are generated via photoexcitation and ionization of H^-: $H^- \rightarrow H^0 + e^-$, there are considerable differences regarding the nature of the excited states in C12A7:H, as we discussed in Sec. IV B, as well as in the mechanism of the conductivity in the postirradiated samples.

The model presented in Refs. 13 and 20 suggests that the extraframework electrons conduct via polaron hopping along continuous chainlike pathways which include 12 hopping sites per unit cell: two encaged OH^- ions, two H^0 atoms, and the *d* states of eight framework Ca^{2+} ions nearest to them[13,20] (but not unoccupied cages[5]). This mechanism requires a high (2.3×10^{21} cm^{-3}) concentration of H^- ions in the preirradiated C12A7:H samples to form such pathways. Experimentally, however, the concentration that has been sufficient to provide measurable uv-induced conductivity is two orders of magnitude smaller (10^{19} cm^{-3}).[14] In contrast, we suggest[5,6] that the electrons hop via states of empty cages, which are

essentially equivalent to each other but perturbed by the extraframework species in occupied cages.

According to Refs. 13 and 20 a high concentration of H^0 atoms is stable in postirradiation samples even at room temperature. However, H^0 atoms have never been detected in samples irradiated at room temperature[18] (see Sec. II B). We note that the H^0+e^- recombination and $O^{2-}+H^0$ reaction channels have not been discussed in Refs. 13 and 20.

VI. DISCUSSION AND CONCLUSIONS

While the existence of protons (as OH^- species) and hydrogen atoms can be addressed experimentally with ir and EPR techniques, respectively, the H^- species are far more elusive because they are EPR inactive and may not be present in concentrations sufficient to be detected with ir spectroscopy. Extensive studies of ir spectra of the MgO surface exposed to H_2 gas suggest that the band at 1130 cm^{-1} should be associated with Mg^{2+}-H^- stretching.[59] In general, however, a cation-H^- stretching can be overshadowed by the lattice vibrations, especially in systems where large concentrations of hydrogenous defects are difficult to achieve. In such cases, theoretical calculations provide a valuable tool for testing the models.

The results presented in this work demonstrate that H^- species are stable in C12A7 and can be formed there as a result of the heterolytic dissociation of H_2 molecules. Furthermore, our calculations suggest that uv-induced generation of extraframework electrons in C12A7 takes place in two basic steps: (i) photoionization of H^-, followed by (ii) thermal ionization of H^0 via its reaction with extraframework O^{2-}. The latter step is essential to suppress the recombination of electrons and H^0 atoms formed during the photoionization step and, thus, to provide stability for the extraframework electrons.

This model is consistent with the results of the photoinduced coloration of C12A7:H reported earlier in Ref. 4. Moreover, recent observations[18] of the temperature dependence of the H^0 concentration in postirradiation C12A7:H are also consistent with the theoretically predicted thermally activated decay of H^0 atoms.[19]

Finally we note that the mechanisms of generation of extraframework electrons in C12A7:H both via photoionization of H^- and via the reaction of atomic H with lattice O^{2-} ions are surprisingly similar to those found for H-treated MgO surfaces. For example, exposure of MgO surfaces to H_2 molecules followed by uv irradiation, as well as exposure of MgO to atomic hydrogen, results in the formation of surface electronic centers in the vicinity of low-coordinated O^{2-} sites (see, for example, Refs. 60–63 and references therein). While the detailed comparative analysis of sites participating in these reactions is beyond the scope of this work, one may suggest that the generation of electronic centers by exposing specific O^{2-} species to atomic hydrogen could be a general phenomenon in oxides.

ACKNOWLEDGMENTS

The authors wish to acknowledge fruitful discussions with S. Matsuishi, J. L. Gavartin, I. V. Abarenkov, M. Sterrer, O. Diwald, G. Pacchioni, E. Giamello, M. Chiesa, and A. M. Stoneham. P.V.S. is grateful to F. Corà, M. Alfredsson, and D. Muñoz Ramo for help with the CRYSTAL program. We are grateful to C. Bird for careful reading of the manuscript. This work was supported by a Grant-in-Aid for Creative Scientific Research (Grant No. 16GS0205) from the Japanese Ministry of Education, Culture, Sports, Science and Technology. The computer time on the HPCx facility was awarded to the Materials Chemistry consortium under EPSRC Grant No. GR/S13422/01. Use of the HiPerSPACE computer facility is also acknowledged.

APPENDIX: THE EXTRAFRAMEWORK ELECTRONS IN THE C12A7 LATTICE

The electronic structure of the dilute concentration of extraframework electrons in C12A7, the nature of their optical absorption and the conductivity mechanism through C12A7 lattice were first reported in Refs. 5 and 6. Two alternative models have recently been put forward on the basis of studies of high extraframework electron concentrations considered using the periodic model and different realizations of the density functional approach.[47,64] It has been suggested in Ref. 64 that these electrons delocalize over the framework but avoid the empty space of the cages. In contrast, results

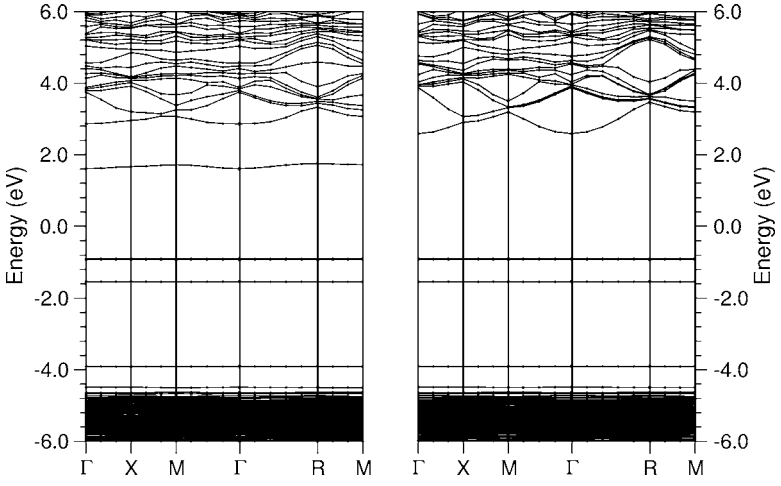

FIG. 7. The band structure calculated for a concentration of one extraframework electron in stoichiometric C12A7: $[Ca_{24}Al_{28}O_{64}]^{4+}\cdot O^{2-}OH^-e^-$. The left and right panels correspond to the spin-up and spin-down states, respectively. (See text for details.)

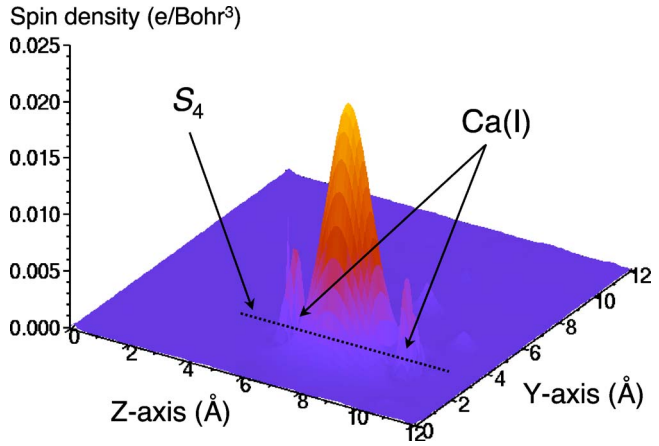

FIG. 8. (Color online) Electron spin density calculated for the C12A7 with a chemical composition of $[Ca_{24}Al_{28}O_{64}]^{4+}\cdot O^{2-}OH^{-}e^{-}$. The spin density peak is centered at approximately $y=3$ Å and $z=7$ Å. The positions of Ca(I) ions for the electron-containing cage and the corresponding S_4 axis are also shown.

reported in Ref. 47 suggest that the electrons avoid the framework and that their density is mostly associated with the middle of the cages and is delocalized over *all* the cages. The comparative analysis of these three models falls beyond the scope of this paper and will be considered elsewhere.[65] Here we describe the results obtained using the periodic model calculations and B3LYP density functional for two combinations of the extraframework species in a unit cell: (i) a single extraframework electron coexisting with O^{2-} and OH^{-} ions, and (ii) four extraframework electrons. The results obtained using the periodic and embedded cluster models are then compared.

The geometry of the cubic unit cell containing extraframework O^{2-}, OH^{-}, and e^{-} species randomly distributed over the 12 cages was optimized at the unrestricted Hartree-Fock (UHF) level of theory and then the electronic structure of the whole system was calculated using the B3LYP density functional.[66] The resulting band structures for spin-up and spin-down states are shown in the left and right panels of Fig. 7, respectively. The top of the valence band is located at approximately −4.5 eV; a single occupied state at −4.0 eV is split from the top of the valence band due to the lattice interaction with extraframework OH^{-}. One of the three $2p$ states associated with the extraframework O^{2-} ions is at −1.6 eV and the other two nearly degenerate states are at −0.8 eV. Finally, the state associated with the extraframework electron is at approximately 1.6 eV, i.e., nearly 6 eV above the top of the VB. This state is split by more than 1 eV from the lowest unoccupied states of the system. The fact that the extraframework electron state in Fig. 7 has almost no dispersion indicates that this is a rather localized state.

Furthermore, the spin density, plotted in the z-y plane that includes both Ca(I) atoms of the electron-containing cage and the corresponding S_4 axis, is shown in Fig. 8. The pronounced maximum of the spin density corresponds to the middle of the cage with coordinates ($y=3$ Å, $z=7$ Å). There are no visible tails of the spin density in other cages. The relative position of the extraframework electron level with respect to the band edges (nearly 6 eV above the top of the VB and over 1 eV below the CB) can be compared to that calculated using the embedded cluster approach for the dilute concentration of electrons (about 4.3 eV above the top of the VB and approximately 1 eV below the unoccupied states of empty cages comprising the cage conduction band). The CCB states obtained in the embedded cluster calculations are split by approximately another 1 eV from the framework conduction band (FCB) states.[6,19] This split, however, is not obvious in the band structure obtained in the periodic calculations (see Fig. 7) perhaps due to the width of the CCB.

The maximum concentration of the extraframework electrons was considered in a similar manner. In this case the extraframework system included four electrons. Again, the internal coordinates of the system were optimized using the UHF approach, followed by a single-point energy calculation using the B3LYP density functional. The band structures calculated for the spin-up and spin-down states with total spin $S=2$ configuration are shown in Fig. 9. One can see that the four occupied states now form a narrow subband at 1.4–2.0 eV, which is still split from the bottom of the cage conduction band at 3.3 eV. The final width together with a noticeable dispersion of the extraframework electrons band indi

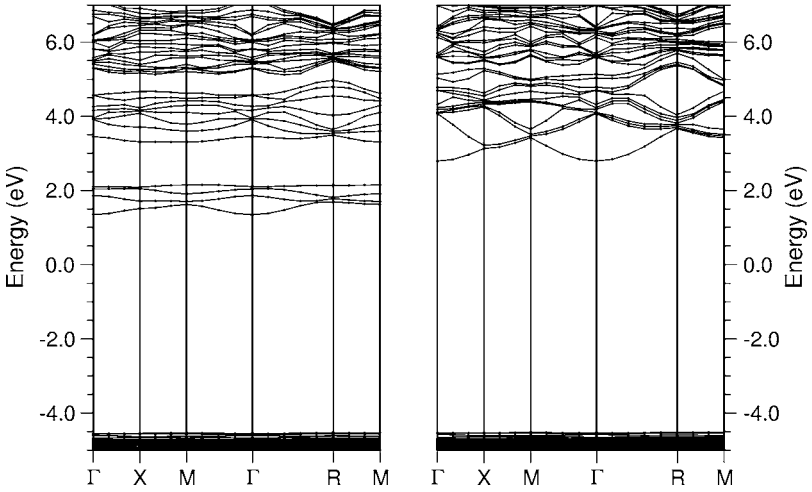

FIG. 9. The band structure calculated for the maximum concentration of four extraframework electrons in stoichiometric C12A7: $[Ca_{24}Al_{28}O_{64}]^{4+}\cdot 4e^{-}$. The left and right panels correspond to the spin-up and spin-down states, respectively. (See text for details.)

cate that the electron states forming it are more delocalized than in the case of the single extraframework electrons. This is consistent with a dramatic increase of the conductivity observed in C12A7 samples at high concentrations of the extraframework electrons.[67] Still, the dispersion of the occupied states is smaller than that of the unoccupied spin-down states of the cage conduction band, which suggests that the extraframework electron density retains its localized character to some extent.

To summarize, both periodic and embedded cluster models suggest that the extraframework electrons are localized in the low-concentration limit and produce consistent electronic structures for this system. Therefore, application of the embedded cluster approach to the investigation of the uv-induced formation of extraframework electrons in Sec. IV is justified. The results presented in this appendix also support our previous reports on the properties of extraframework electrons in C12A7.[5,6]

*Corresponding author. Email address: p.sushko@ucl.ac.uk

[1] S. F. Cox, J. Phys.: Condens. Matter **15**, R1727 (2003).
[2] C. G. V. de Walle and J. Neugebauer, Nature (London) **423**, 626 (2003).
[3] C. Kilic and A. Zunger, Appl. Phys. Lett. **81**, 73 (2002).
[4] K. Hayashi, S. Matsuishi, T. Kamiya, M. Hirano, and H. Hosono, Nature (London) **419**, 462 (2002).
[5] P. V. Sushko, A. L. Shluger, K. Hayashi, M. Hirano, and H. Hosono, Phys. Rev. Lett. **91**, 126401 (2003).
[6] P. V. Sushko, A. L. Shluger, K. Hayashi, M. Hirano, and H. Hosono, Thin Solid Films **445**, 161 (2003).
[7] J. A. Imlach, L. S. D. Glasser, and F. P. Glasser, Cem. Concr. Res. **1**, 57 (1971).
[8] S. Wataushi, I. Tanaka, K. Hayashi, M. Hirano, and H. Hosono, J. Cryst. Growth **237**, 496 (2002).
[9] K. Hayashi, M. Hirano, S. Matsuishi, and H. Hosono, J. Am. Chem. Soc. **124**, 738 (2002).
[10] K. Hayashi, S. Matsuishi, M. Hirano, and H. Hosono, J. Phys. Chem. B **108**, 8920 (2004).
[11] S. Matsuishi, K. Hayashi, M. Hirano, I. Tanaka, and H. Hosono, J. Phys. Chem. B **108**, 18557 (2004).
[12] J. Jeevaratnam, F. P. Glasser, and L. S. D. Glasser, J. Am. Ceram. Soc. **47**, 105 (1964).
[13] J. E. Medvedeva, A. J. Freeman, M. I. Bertoni, and T. O. Mason, Phys. Rev. Lett. **93**, 016408 (2004).
[14] M. Miyakawa, K. Hayashi, M. Hirano, Y. Toda, T. Kamiya, and H. Hosono, Adv. Mater. (Weinheim, Ger.) **15**, 1100 (2003).
[15] Y. Toda, M. Miyakawa, K. Hayashi, T. Kamiya, M. Hirano, and H. Hosono, Thin Solid Films **445**, 309 (2003).
[16] M. Miyakawa, Y. Toda, K. Hayashi, M. Hirano, T. Kamiya, N. Matsunami, and H. Hosono, J. Appl. Phys. **97**, 023510 (2005).
[17] K. Hayashi, Y. Toda, T. Kamiya, M. Hirano, M. Yamanaka, I. Tanaka, T. Yamamoto, and H. Hosono, Appl. Phys. Lett. **86**, 022109 (2005).
[18] S. Matsuishi, K. Hayashi, M. Hirano, and H. Hosono, J. Am. Chem. Soc. **127**, 12454 (2005).
[19] P. V. Sushko, A. L. Shluger, K. Hayashi, M. Hirano, and H. Hosono, Appl. Phys. Lett. **86**, 092101 (2005).
[20] M. I. Bertoni, T. O. Mason, J. E. Medvedeva, A. J. Freeman, K. R. Poeppelmeier, and B. Delley, J. Appl. Phys. **97**, 103713 (2005).
[21] G. Kresse and J. Furthmüller, Phys. Rev. B **54**, 11169 (1996).
[22] J. P. Perdew and Y. Wang, Phys. Rev. B **46**, 12947 (1992).
[23] P. E. Blöchl, Phys. Rev. B **50**, 17953 (1994).
[24] G. Kresse and D. Joubert, Phys. Rev. B **59**, 1758 (1999).
[25] M. Lacerda, J. T. S. Irvine, F. P. Glasser, and A. R. West, Nature (London) **332**, 525 (1988).
[26] P. V. Sushko, A. L. Shluger, and C. R. A. Catlow, Surf. Sci. **450**, 153 (2000).
[27] B. G. Dick and A. W. Overhauser, Phys. Rev. **112**, 90 (1958).
[28] V. B. Sulimov, P. V. Sushko, A. H. Edwards, A. L. Shluger, and A. M. Stoneham, Phys. Rev. B **66**, 024108 (2002).
[29] J. S. Braithwaite, P. V. Sushko, K. Wright, and C. R. A. Catlow, J. Chem. Phys. **116**, 2628 (2002).
[30] P. V. Sushko, J. L. Gavartin, and A. L. Shluger, J. Phys. Chem. B **106**, 2269 (2002).
[31] S. Mukhopadhyay, P. V. Sushko, A. M. Stoneham, and A. L. Shluger, Phys. Rev. B **70**, 195203 (2004).
[32] M. O. Zacate and R. W. Grimes, J. Phys. Chem. Solids **63**, 675 (2002).
[33] M. J. Frisch *et al.*, Computer code GAUSSIAN 98 Revision A.7 (Gaussian Inc., Pittsburgh, PA, 1998).
[34] A. D. Becke, J. Chem. Phys. **98**, 5648 (1993).
[35] C. Lee, W. Yang, and R. G. Parr, Phys. Rev. B **37**, 785 (1988).
[36] J. Muscat, A. Wander, and N. M. Harrison, Chem. Phys. Lett. **342**, 397 (2001).
[37] W. R. Wadt and P. J. Hay, J. Chem. Phys. **82**, 284 (1985).
[38] P. J. Hay and W. R. Wadt, J. Chem. Phys. **82**, 299 (1985).
[39] V. R. Saunders *et al.*, *Computer code CRYSTAL2003 User's Manual* (University of Torino, Torino, 2003).
[40] http://www.crystal.unito.it/Basis-Sets/ptable.html
[41] T. Ito, M. Kuramoto, M. Yoshioka, and T. Tokuda, J. Phys. Chem. **87**, 4411 (1983).
[42] A. L. Shluger, J. D. Gale, and C. R. A. Catlow, J. Phys. Chem. **96**, 10389 (1992).
[43] M. Sterrer, T. Berger, O. Diwald, E. Knözinger, P. V. Sushko, and A. L. Shluger, J. Chem. Phys. **123**, 064714 (2005).
[44] B. C. Schmidt, F. M. Holtz, and J. M. Beny, J. Non-Cryst. Solids **240**, 91 (1998).
[45] S. Bordiga, E. Garrone, C. Lambert, A. Zecchina, C. O. Arean, V. B. Kazansky, and L. M. Kustov, J. Chem. Soc., Faraday Trans. **90**, 3367 (1994).
[46] J. Eckert, J. M. Nicol, J. Howard, and F. R. Trouw, J. Phys. Chem. **100**, 10646 (1996).
[47] Z. Li, J. Yang, J. G. Hou, and Q. Zhu, Angew. Chem., Int. Ed. **43**, 6479 (2004).
[48] G. Pacchioni, F. Frigoli, D. Ricci, and J. A. Weil, Phys. Rev. B **63**, 054102 (2001).
[49] J. L. Gavartin, P. V. Sushko, and A. L. Shluger, Phys. Rev. B **67**, 035108 (2003).
[50] J. To, A. A. Sokol, S. A. French, N. Kaltsoyannis, and C. R. A. Catlow, J. Chem. Phys. **122**, 144704 (2005).

[51] D. Munoz, N. M. Harrison, and F. Illas, Phys. Rev. B **69**, 085115 (2004).
[52] X. Liu, G. Zhang, and J. K. Thomas, J. Phys. Chem. B **101**, 2182 (1997).
[53] M. Gutowski, C. S. Hall, L. Adamowicz, J. H. Hendricks, H. L. de Clercq, S. A. Lyapustina, J. M. Nilles, S.-J. Xu, and K. H. Bowen, Phys. Rev. Lett. **88**, 143001 (2002).
[54] The relaxed configuration of the lowest excited singlet was approximated by the relaxed configuration of the corresponding triplet state, i.e., the ground state in the triplet domain.
[55] K. Kajihara, L. Skuja, M. Hirano, and H. Hosono, Phys. Rev. Lett. **89**, 135507 (2002).
[56] B. Tuttle, Phys. Rev. B **61**, 4417 (2000).
[57] M. Lacerda, A. R. West, and J. T. S. Irvine, Solid State Ionics **59**, 257 (1993).
[58] K. Hayashi, P. V. Sushko, A. L. Shluger, M. Hirano, and H. Hosono, J. Phys. Chem. B **109**, 23836 (2005).
[59] O. Diwald, P. Hofmann, and E. Knözinger, Phys. Chem. Chem. Phys. **1**, 713 (1999).
[60] M. C. Paganini, M. Chiesa, E. Giamello, S. Coluccia, G. Martra, D. M. Murphy, and G. Pacchioni, Surf. Sci. **421**, 246 (1999).
[61] D. Ricci, C. D. Valentin, G. Pacchioni, P. V. Sushko, A. L. Shluger, and E. Giamello, J. Am. Chem. Soc. **125**, 738 (2003).
[62] T. Berger, M. Sterrer, O. Diwald, and E. Knözinger, J. Phys. Chem. B **108**, 7280 (2004).
[63] M. Chiesa, M. C. Paganini, G. Spoto, E. Giamello, C. D. Valentin, A. D. Vitto, and G. Pacchioni, J. Phys. Chem. B **109**, 7314 (2005).
[64] J. E. Medvedeva and A. J. Freeman, Appl. Phys. Lett. **85**, 955 (2004).
[65] P. V. Sushko, A. L. Shluger, K. Hayashi, M. Hirano, and H. Hosono (unpublished).
[66] We used such a combination of methods so as to reduce the computational cost of the calculations. We, however, checked that the details of the local geometry do not significantly affect the overall electronic structure of the system.
[67] S. Matsuishi, Y. Toda, M. Miyakawa, K. Hayashi, T. Kamiya, M. Hirano, I. Tanaka, and H. Hosono, Science **301**, 626 (2003).
[68] P. V. Sushko, A. L. Shluger, K. Hayashi, M. Hirano, and H. Hosono, Phys. Rev. B **73**, 014101 (2006).